

Article history: Received 13 August 2025 Revised 23 October 2025 Accepted 04 November 2025 Published online 01 January 2026

Journal of Resource Management and Decision Engineering

Volume 5, Issue 1, pp 1-11



Design of an Optimized Array Antenna in the 64–84 GHz Frequency Band for Application in Autonomous Vehicles

Hamidreza. Rabiee¹, Omid. Rahmani Seryasat^{2*}

¹ Department of Electrical Engineering, Ka.C. Islamic Azad University, Karaj, Iran
² Assistant Professor, Department of Electrical Engineering, Shams Higher Education Institute, Gorgan, Iran

* Corresponding author email address: orseryasat@shamsgonbad.ac.ir

Article Info

Article type:

Original Research

How to cite this article:

Rabiee, H. & Rahmani Seryasat, O. (2026). Design of an Optimized Array Antenna in the 64–84 GHz Frequency Band for Application in Autonomous Vehicles. *Journal of Resource Management and Decision Engineering*, 5(1), 1-11.

https://doi.org/10.61838/kman.jrmde.5.1.201



© 2026 the authors. Published by KMAN Publication Inc. (KMANPUB). This is an open access article under the terms of the Creative Commons Attribution-NonCommercial 4.0 International (CC BY-NC 4.0) License.

ABSTRACT

Automotive radar systems require antennas with specific characteristics to achieve optimal performance. One of the main challenges in this field is reducing signal interference and improving beam steering. In this study, a planar array antenna for millimeter-wave automotive radar applications is proposed, which is capable of meeting these requirements. The antenna consists of thirteen array elements with a linear series feed and a coaxial feeding network. Series-fed microstrip patch array antennas are popular options for millimeter-wave radar applications due to their simple structure, high gain, and low cost. However, the limited impedance bandwidth remains one of the main challenges in designing such antennas. In this research, by employing specific techniques in array and transmission line design, not only is the impedance bandwidth increased, but the sidelobe level is also reduced and beam steering is significantly improved. Simulation results demonstrate a maximum sidelobe level of -13 dB in the E-plane and -10 dB in the H-plane. Additionally, an impedance bandwidth of 20 GHz and a gain higher than 14 dB are achieved.

Keywords: Automotive radar, low sidelobe level (SLL), array antenna, microstrip antenna.

1. Introduction

The emergence of autonomous vehicles has introduced new requirements and challenges for millimeter-wave automotive radar technology (Ahmad et al., 2021; Engels et al., 2017; Harter et al., 2016; Hasch et al., 2012; Ku et al., 2014; Menzel & Moebius, 2012). Among these, the definition of the 76–81 GHz operating frequency range for automotive radars classifies them according to detection range into three main categories: long-range radar (LRR),

mid-range radar (MRR), and short-range radar (SRR) (Pimentel, 2017). The frequency band of 77–81 GHz is primarily used in MRR and SRR systems. Compared with 24 GHz automotive radars, these systems offer higher resolution and smaller size, making them promising for intelligent transportation applications such as adaptive cruise control (ACC), blind-spot detection (BSD), and crosstraffic alert (CTA). To compensate for path loss and extend detection range, designing antenna arrays with high gain is essential. Moreover, minimizing signal interference requires



achieving a low sidelobe level (SLL). Therefore, selecting antenna arrays that offer low SLL, high gain, and reasonable cost is of vital importance in automotive radar systems.

Over the past decade, considerable efforts have been devoted to developing automotive radar antennas. Linear arrays have received particular attention, and researchers have explored various options, including patch arrays, grid antennas, and comb-line arrays. Among these, the SLL index, which indicates the system's anti-interference capability, is of particular importance.

Grid and comb-line arrays, despite their advantages, typically exhibit high SLL due to the difficulty of suppressing sidelobes. In contrast, series-fed patch antenna arrays can provide lower SLL. For example, one study reported a microstrip patch array using a series feed and a differential evolution algorithm achieving an SLL of -25 dB. However, that design neglected mutual coupling between elements, which may not be suitable for very high frequencies such as 79 GHz.

Therefore, optimizing SLL while accounting for mutual coupling between elements—especially high frequencies—is crucial in automotive radar antenna design. In the existing literature, extensive research has focused on designing antenna arrays with reduced sidelobe radiation. For instance, (Chopra & Kumar, 2019) presented linear and planar binomial patch arrays employing a series-feed approach and reduced element width, achieving SLL values below -28 dB. Series-fed patch arrays with low feed loss in the microwave band have also been investigated in (Chopra & Kumar, 2019; Khalili et al., 2018; Yin et al., 2017). However, as the design moves toward the W-band, the shorter wavelength increases design complexity. To address this, the Radiated-to-Available Power Ratio (RAPA) design approach introduced in (Kang et al., 2020) utilized three different types of patch antennas to realize a series-fed linear array with very low SLL, achieving levels below -17 dB across its operational band.

Nevertheless, a major limitation of the existing methods is that they focus solely on SLL optimization without simultaneously optimizing S11 and SLL. In contrast, (Menzel & Moebius, 2012) presented a high-gain array operating at 77 GHz with a half-power beamwidth (HPBW) of 15.63° in the E-plane and 13.6° in the H-plane. However, its -15 dB impedance bandwidth was limited to only 730 MHz. A 77 GHz linear array reported in (Chopra & Kumar, 2019; Kang et al., 2020; Yin et al., 2017) achieved high gain with relative ease. For instance, (Yin et al., 2017) obtained a gain of 12.7 dBi and an SLL of -17.5 dB, while (Kang et al.,

2020) demonstrated similar performance with 16.6 dBi gain and -17.2 dB SLL. However, the main drawback of these arrays is their narrow bandwidth. For example, the -10 dB impedance bandwidth of the array proposed in (Yin et al., 2017) was only 2.5 GHz, whereas the linear array in (Kang et al., 2020) had a bandwidth of 2.91 GHz. The dual-band array reported in (Chopra & Kumar, 2019) operated at 77 GHz and 97 GHz and delivered high gains, yet still suffered from narrow bandwidth. This bandwidth limitation is largely attributed to the microstrip patch antennas used in these arrays (Arnieri et al., 2018; Khalili et al., 2018).

The main objective of this study is to enhance the bandwidth of such arrays without compromising their other desirable features. This paper proposes a series-fed microstrip patch array antenna offering a wide impedance bandwidth and effective sidelobe suppression across the 64–84 GHz frequency range. Electromagnetic simulations conducted using the commercial CST software demonstrate that the proposed array achieves an impedance bandwidth of 20 GHz.

2. Theoretical Analysis of the Proposed Antenna Performance

The primary radiating element in a microstrip comb-line antenna array is the open-ended microstrip line. Understanding the radiation mechanism of this element is essential before designing the comb-line array. Therefore, this section examines the electromagnetic radiation process from the open-ended microstrip line.

2.1. Structures and Configurations Used

Figure 1 illustrates a microstrip comb-line antenna array composed of open-ended microstrip lines. These open-ended lines act as the radiating elements of the array. As shown in the figure, the comb-line array is formed by connecting open stubs to a feed line. A detailed analysis of this type of antenna array is presented in this section.

Figure 1

A microstrip comb-line antenna array composed of open-ended stubs.

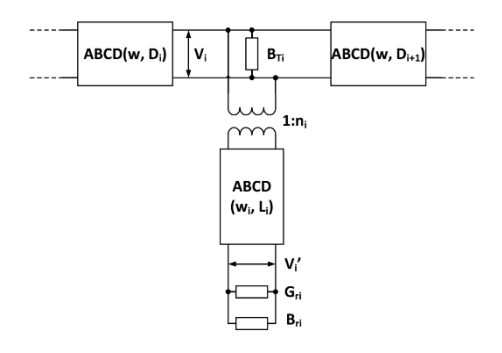




The comb-line antenna shown in Figure 1 can be regarded as a combination of several T-junctions. Figure 2 presents the equivalent circuit of a T-junction, which includes a transformer with a turns ratio of n_i and a susceptance jB_T_i . The feed line and open-line sections surrounding the T-junction are represented using ABCD matrices, while the radiation from the line is characterized by the input admittance parameters $Y_{ri} = G_{ri} + jB_{ri}$ at the terminal port.

Figure 2

Equivalent circuit of a T-junction in a microstrip comb-line



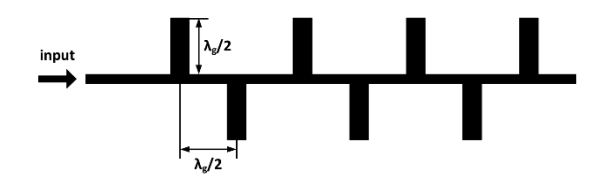
2.2. Comparison Between Traveling-Wave and Standing-Wave Arrays

To achieve array phase coherence at the target frequency, in Figure 1, the spacing between adjacent lines is chosen to be equal to one wavelength. The weakness of this configuration lies in its grating lobes. A simple solution is to alternately place the stubs on both sides of the feed line, as shown in Figure 3. This new arrangement changes both the line spacing and the line length to half a wavelength. Consequently, the input received through the feed line equals the radiated input at the line's open end.

The end of the feed line represents a point where a traveling-wave array is formed using a matched load termination. These arrays belong to the family of microstrip comb-line antenna arrays, which are classified according to their termination type into *traveling-wave* and *standing-wave* arrays. In such arrays, the main power is gradually radiated along the lines and eventually dissipated at the matched load.

Figure 3

A microstrip comb-line antenna array with half-wavelength line spacing.



3. Design of the Proposed Antenna

Among the commercially available software packages for antenna design, HFSS and CST are the most widely used and preferred. Both tools are capable of handling complex structures and, when properly configured, deliver high accuracy. In the present research, the CST electromagnetic simulator was used to model and analyze the performance of the proposed antenna. The use of CST's powerful solver enables the achievement of precise and reliable simulation results.

3.1. Design of the Proposed Antenna with 90-Degree Elements

Figure 5 illustrates a comb-line microstrip antenna array configured in a standing-wave arrangement at a 90-degree orientation. As previously mentioned, both the open-ended microstrip line length and the spacing between adjacent lines are equal to half the wavelength. In this design, the array's amplitude distribution is achieved by controlling the width of each open stub. In the simple uniform array case, all stubs have equal width to provide uniform power distribution across the aperture.

The entire microstrip structure is implemented on a substrate operating at 76.5 GHz, with a relative dielectric constant of 3.2 and a loss tangent of 0.0168. These parameters were obtained empirically, as the values specified in the datasheet are valid only for much lower frequencies.

Figure 4 shows the schematic of the substrate structure, which is enclosed by two conductive layers—an upper radiating patch and a lower ground plane. Due to manufacturing constraints, the minimum achievable line width is 0.10 mm.

Figure 4

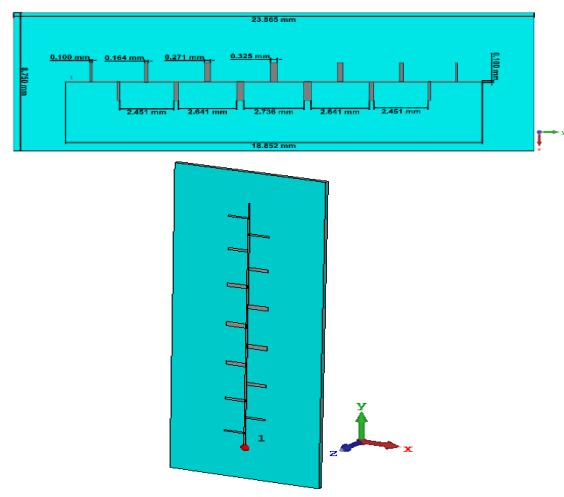
Schematic cross-sectional view of the antenna layers.



Figure 5 presents the complete antenna with perpendicular arms and its dimensions. The antenna design consists of a central microstrip feed line connected to thirteen 90-degree arms. This optimized configuration enhances the antenna's performance and distinguishes it from conventional designs.

Figure 5

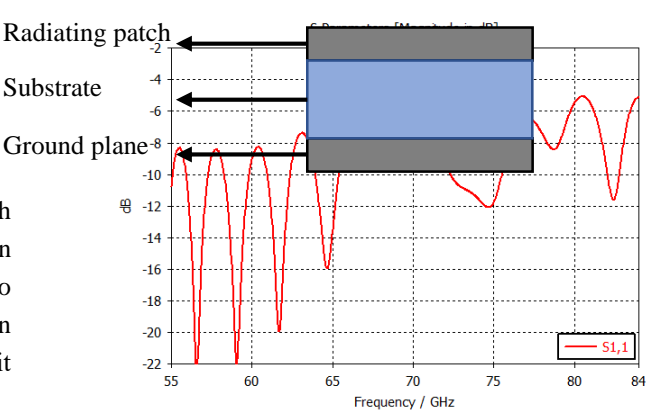
A microstrip comb-line antenna array with half-wavelength line spacing.



The proposed antenna's arms play a crucial role in its radiation characteristics. The antenna is fed through a 50- Ω coaxial probe. The scattering parameter (S-parameter) plot of the antenna, shown below, provides important information about its operating frequency. According to Figure 6, the operating frequency range fluctuates between 55 GHz and 84 GHz, indicating an insufficient bandwidth. This frequency span only partially covers the desired range. To improve bandwidth, in the next stage, the arm angles will be modified to enhance the antenna's performance.



 $S11\ scattering\mbox{-parameter plot of the proposed antenna}\ (Figure\ 5).$



The antenna radiation pattern is shown in Figure 7, displaying the power distribution at various frequencies. The figure indicates that the antenna exhibits excellent directivity. Furthermore, the low sidelobe level (SLL) observed in Figure 7 confirms the antenna's favorable performance in minimizing signal interference.

Figure 7

Radiation-pattern diagram of the proposed antenna (Figure 5).

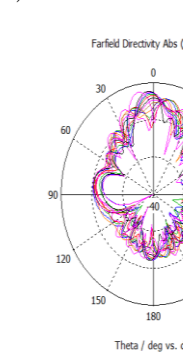


Figure 8 shows the VSWR characteristics of the antenna, demonstrating the effectiveness of the design. As the frequency increases, the VSWR approaches its ideal value, confirming the antenna's high quality and its capability to operate efficiently across a wide frequency range.

Figure 8

Figure 8. VSWR curve of the proposed antenna (Figure 5).



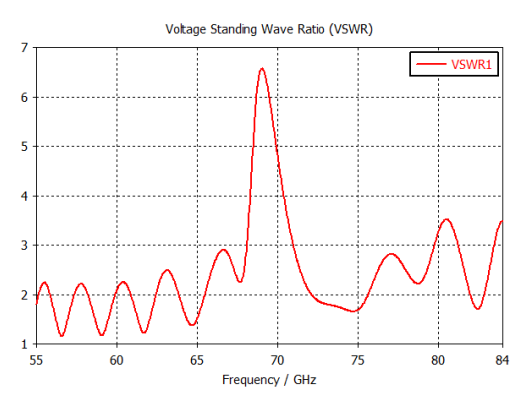
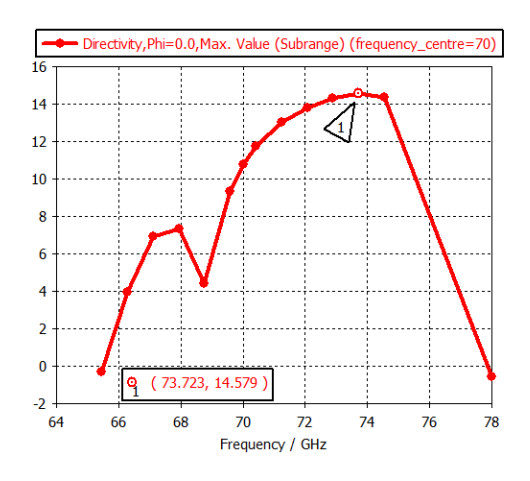


Figure 9 presents the antenna gain across its operational frequencies. The peak gain occurs in the 72–73 GHz range, reaching 14.57 dB.

Figure 9

Gain response of the proposed antenna over its operational

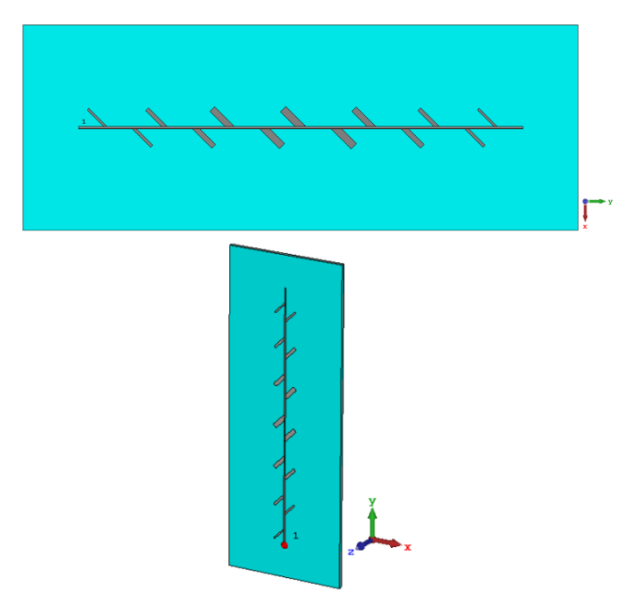


3.2. Design of the Proposed Antenna with 45-Degree Elements

At this stage, to achieve higher operational frequencies and shift the working range to 70–84 GHz, the 90-degree arms were redesigned to 45-degree angles. This redesign resulted in an upward frequency shift, allowing the antenna to reach the desired operational range. Figure 10 illustrates the final antenna design incorporating these modifications, confirming the successful redesign in achieving the target frequency specifications.

Figure 10

Redesigned antenna with 45-degree arms.



By changing the arm angle from 90° to 45°, the antenna's operating frequency increased and aligned more closely with the desired frequency band. Figure 10 again shows the final design, validating the effectiveness of this optimization.

Figure 11 presents the S11 scattering-parameter plot for the redesigned antenna. The radiation-pattern plots in Figure 12 depict the antenna's behavior across multiple frequencies, showing significantly improved directivity compared with conventional 90-degree designs.

Figure 11
S11 scattering-parameter plot of the redesigned antenna (Figure 10).

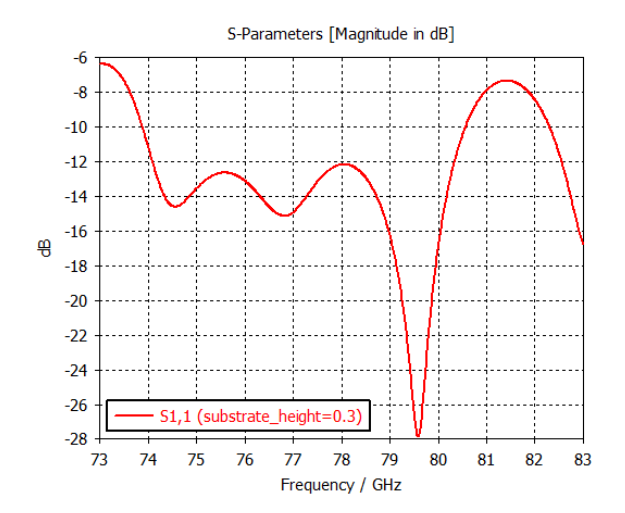


Figure 12

Radiation-pattern diagram of the redesigned antenna (Figure 10).

frequencies.



Furfield Directority Also (Phi=0)

zed on a

zed on a

tangent

individ (P-2.23) (substrate, longer-0.3)

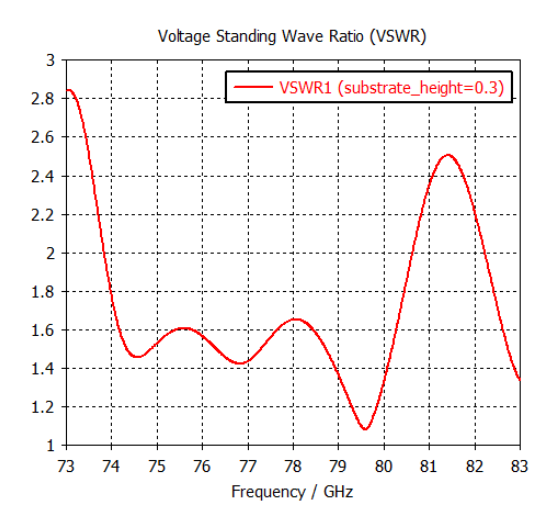
individ

uscu in the proposed array amenina is mustrated in 1 igure 14.

Figure 13 shows the VSWR performance of the proposed antenna. The results reveal that as the operating frequency increases, the antenna's impedance purity also improves, confirming its stable and accurate behavior. Furthermore, all operating frequencies maintain VSWR values below 2 dB, indicating an excellent impedance match.

Figure 13

VSWR curve of the redesigned antenna (Figure 10).



4. Feed Network Design

Considering the necessity of array integration for the single-element antenna proposed in previous studies, designing an appropriate feed network is essential. It is well known that conventional feed networks suffer from narrow bandwidth. Therefore, to achieve a broader operational bandwidth in this study, it was necessary to design a feed network with an extended bandwidth capability.

The bandwidth of a conventional Wilkinson power divider is inherently limited to less than 5 GHz. However, a method proposed in the literature significantly enhances bandwidth by increasing the number of Wilkinson divider stages (Bauer & Menzel, 2013a; Bauer et al., 2013; Wang & Stelzer, 2013). This technique connects multiple Wilkinson dividers in cascade, with each stage tuned such that their resonance frequencies overlap, resulting in a single combined resonance with a much wider bandwidth.

Figure 14

Geometry of the designed two-stage 1:2 Wilkinson feed line.

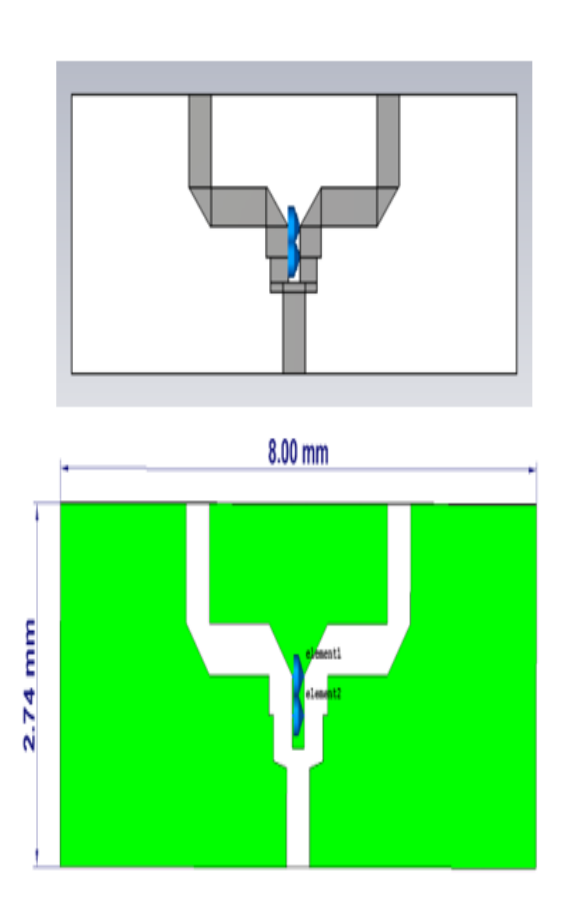
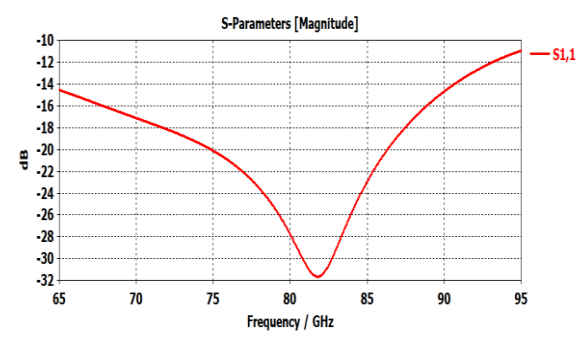


Figure 15 shows the return-loss curve for the input port of the two-stage 1:2 Wilkinson power divider integrated into the proposed array. The measured reflection response confirms a well-matched impedance and effective power distribution across the feeding network.

Figure 15

Return-loss plot of the input port for the two-stage 1:2 Wilkinson power divider used in the proposed array antenna.





Based on the results presented, the feed network was successfully designed for the proposed antenna. The next section presents the analysis of this design to evaluate its overall performance and compatibility with the antenna array system.

5. Design of the Array Antenna

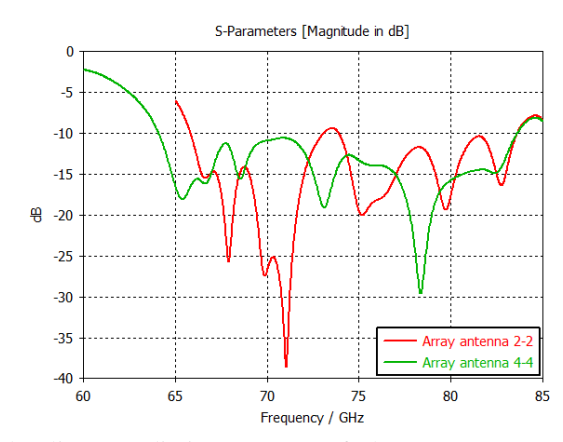
By combining the single-element antenna and the feeding network introduced in the previous sections, an array antenna was developed to enhance bandwidth and directivity. The proposed array was designed and analyzed in two configurations: a two-element array and a four-element array. Figure 16 presents both configurations along with the detailed feeding line layout.

Figure 16

Two-element and four-element array antenna configurations with integrated feed lines.

Figure 17

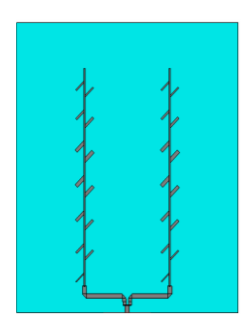
Comparative S-parameter chart of two- and four-element array antennas with feed network integration.



The linear radiation pattern of the antenna array is illustrated in Figure 18. The figure shows that the four-element array provides superior directivity and higher antenna gain. This improvement leads to reduced sidelobe levels, which in turn enhances obstacle detection accuracy and improves data transmission reliability in autonomous vehicle radar systems.

Figure 18

Linear radiation pattern of the proposed array antenna.



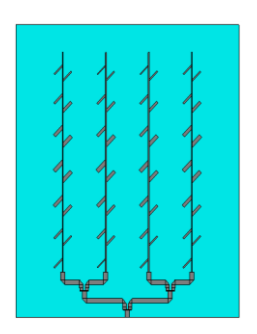




Figure 17 shows the S-parameter comparison for both array configurations. The plot clearly indicates that the four-element array exhibits a much broader impedance bandwidth compared with the single-element and two-element arrays. This finding demonstrates the considerable advantage of four-element array structures in applications demanding wide bandwidth.

Figure 19 visualizes the surface current distribution for both two-element and four-element configurations. As observed, the feed line is designed to distribute current uniformly across the array, demonstrating the electrical balance and stability of the proposed design.



Figure 19
Surface current distribution in the two-element and four-element array configurations.

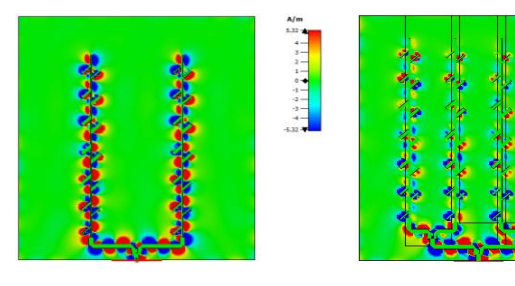


 Table 1

 Comparison of the Proposed Antenna with Previous Works

| Number of Elements | SLL (dB) | Gain (dB) | Frequency (GHz) | Reference |
|--------------------|----------|-----------|-----------------|--------------------------------|
| 1×16 | -12.5 | 8.5 | 77–81 | (Wang & Stelzer, 2013) |
| 1×2 | -12 | 6.5 | 77–81.5 | (Lu et al., 2019) |
| 4×7 | -10 | 10 | 76–81 | (Kehn et al., 2022) |
| 2×5 | -15.9 | 11.5 | 77–79 | (Yoo et al., 2020) |
| 1×5 | -14 | 10.5 | 77–79 | (Mosalanejad et al., 2018) |
| 2×13 | -15 | 9.5 | 77 | (Galvis Salzburg et al., 2018) |
| 1×10 | -16 | 12.4 | 77–80 | (Bauer & Menzel, 2013b) |
| 1×12 | -17 | 9.6 | 78–80 | (Bauer & Menzel, 2013a) |
| 1×8 | -14 | 13.2 | 74–82 | (Khan et al., 2017) |
| 1×4 | -10 | 11 | 75.7-84.8 | (Mosalanejad et al., 2019) |
| 2×4 | -13 | 11.6 | 77–81 | (Saleem et al., 2017) |
| 1×17 | -10 | 13.05 | 77–81 | (Pimentel, 2017) |
| 4×13 | -21.5 | 14 | 64–84 | This work |

Table 1 presents a comprehensive comparison of various parameters—frequency range, gain, sidelobe level (SLL), and number of elements—between the proposed antenna and previous designs reported in the literature. The results indicate that the antenna introduced in this study demonstrates a significant advancement over prior designs, particularly in terms of gain enhancement, wider bandwidth, and improved sidelobe suppression.

6. Conclusion

In this paper, the theory and design of a horn-type array antenna were analyzed and developed. Using electromagnetic wave simulation software, the antenna structures were modeled and their analytical results extracted. The simulation process was conducted in two stages: first, the design of the single-element antenna; and second, the integration of multiple antennas into an array system along with the feed network.

The primary objectives in autonomous vehicle radar antennas are achieving precise beam direction and minimizing sidelobes, as high detection accuracy and rapid data transmission are critical for these systems. Based on the findings of this research, by arraying the antennas within a 20 GHz bandwidth, a gain of 14 dB was achieved. These results confirm that the proposed antenna array is both suitable and efficient for automotive radar applications in the 64–84 GHz frequency band.

Authors' Contributions

Authors contributed equally to this article.

Declaration

In order to correct and improve the academic writing of our paper, we have used the language model ChatGPT.

Transparency Statement

Data are available for research purposes upon reasonable request to the corresponding author.

Acknowledgments



We would like to express our gratitude to all individuals helped us to do the project.

Declaration of Interest

The authors report no conflict of interest.

Funding

According to the authors, this article has no financial support.

Ethics Considerations

In this research, ethical standards including obtaining informed consent, ensuring privacy and confidentiality were considered.

References

- Ahmad, W. A., Kucharski, M., Ergintav, A., Ng, H. J., & Kissinger, D. A. (2021). Planar Differential Wide Fan-Beam Antenna Array Architecture: Modular high-gain array for 79-GHz multiple-input, multiple-output radar applications. *IEEE Antennas and Propagation Magazine*, 63(1), 21-23. https://doi.org/10.1109/MAP.2020.2976913
- Arnieri, A., Greco, F., Boccia, L., & Amendola, G. (2018). A Reduced Size Planar Grid Array Antenna for Automotive Radar Sensors. *IEEE Antennas and Wireless Propagation Letters*, 17(12), 2389-2393. https://doi.org/10.1109/LAWP.2018.2876150
- Bauer, F., & Menzel, W. (2013a). A 79-GHz planar antenna array using ceramic-filled cavity resonators in LTCC. *IEEE Antennas and Wireless Propagation Letters*, 12, 910-913. https://doi.org/10.1109/LAWP.2013.2272914
- Bauer, F., & Menzel, W. (2013b). A 79-GHz resonant laminated waveguide slotted array antenna using novel shaped slots in LTCC. IEEE Antennas and Wireless Propagation Letters, 12, 296-299. https://doi.org/10.1109/LAWP.2013.2248694
- Bauer, F., Wang, X., Menzel, W., & Stelzer, A. (2013). A 79-GHz radar sensor in LTCC technology using grid array antennas. *IEEE Transactions on Microwave Theory and Techniques*, 61(6), 2514-2514. https://doi.org/10.1109/TMTT.2013.2260766
- Chopra, R., & Kumar, G. (2019). Series-Fed Binomial Microstrip Arrays for Extremely Low Sidelobe Level. *IEEE Transactions* on Antennas and Propagation, 67(7), 4275-4279. https://doi.org/10.1109/TAP.2019.2908108
- Engels, F., Heidenreich, P., Zoubir, A. M., Jondral, F. K., & Wintermantel, M. (2017). Advances in Automotive Radar: A framework on computationally efficient high-resolution frequency estimation. *IEEE Signal Processing Magazine*, 34(2), 36-46. https://doi.org/10.1109/MSP.2016.2637700
- Galvis Salzburg, C., Vaupel, T., Bertuch, T., Wilhelm, M., Wichmann, T., & Tejero Alfageme, S. (2018). Feasibility of an automotive radar antenna at 77 GHz on LTCC substrate. *IET Radar, Sonar & Navigation*, 12(10), 1172-1178. https://doi.org/10.1049/iet-rsn.2018.5018
- Harter, M., Hildebrandt, J., Ziroff, A., & Zwick, T. (2016). Self-Calibration of a 3-D-Digital Beamforming Radar System for Automotive Applications with Installation Behind

- Automotive Covers. *IEEE Transactions on Microwave Theory and Techniques*, 64(9), 2994-3000. https://doi.org/10.1109/TMTT.2016.2593731
- Hasch, J., Topak, E., Schnabel, R., Zwick, T., Weigel, R., & Waldschmidt, C. (2012). Millimeter-Wave Technology for Automotive Radar Sensors in the 77 GHz Frequency Band. *IEEE Transactions on Microwave Theory and Techniques*, 60(3), 845-860. https://doi.org/10.1109/TMTT.2011.2178427
- Kang, Y., Noh, E., & Kim, K. (2020). Design of Traveling-Wave Series-Fed Microstrip Array with a Low Sidelobe Level. *IEEE Antennas and Wireless Propagation Letters*, 19(8), 1395-1399. https://doi.org/10.1109/LAWP.2020.2989916
- Kehn, M. N. M., Rajo-Iglesias, E., & Yang, T. C. (2022). W-band 76-81 GHz millimeter-wave comb-line array for automotive short range radar. *Radio Science*, 57(4). https://doi.org/10.1029/2021RS007407
- Khalili, H., Mohammadpour-Aghdam, K., Alamdar, S., & Mohammad-Taheri, M. (2018). Low-Cost Series-Fed Microstrip Antenna Arrays with Extremely Low Sidelobe Levels. *IEEE Transactions on Antennas and Propagation*, 66(9), 4606-4612. https://doi.org/10.1109/TAP.2018.2845442
- Khan, O., Meyer, J., Baur, K., & Waldschmidt, C. (2017). Hybrid thin film antenna for automotive radar at 79 GHz. *IEEE Transactions on Antennas and Propagation*, 65(10), 5076-5085. https://doi.org/10.1109/TAP.2017.2741024
- Ku, B. H., Schmalenberg, P., Inac, O., Gurbuz, O. D., Lee, J. S., Shiozaki, K. J., & Rebeiz, G. M. (2014). A 77-81-GHz 16-Element Phased-Array Receiver With ±50° Beam Scanning for Advance Automotive Radars. *IEEE Transactions on Microwave Theory and Techniques*, 62(11), 2823-2832. https://doi.org/10.1109/TMTT.2014.2354134
- Lu, Y. J., Chiu, S. C., & Wu, W. Z. (2019). Novel Antenna-in-Package Design for Automotive Surround-View Radar Systems. 2019 Electrical Design of Advanced Packaging and Systems (EDAPS),
- Menzel, M., & Moebius, A. (2012). Antenna Concepts for Millimeter-Wave Automotive Radar Sensors. *Proceedings of the IEEE*, 100(7), 2372-2379. https://doi.org/10.1109/JPROC.2012.2184729
- Mosalanejad, M., Ocket, I., Soens, C., & Vandenbosch, G. A. (2018). Multilayer compact grid antenna array for 79 GHz automotive radar applications. *IEEE Antennas and Wireless Propagation Letters*, *17*(9), 1677-1681. https://doi.org/10.1109/LAWP.2018.2862946
- Mosalanejad, M., Ocket, I., Soens, C., & Vandenbosch, G. A. (2019). Multi-layer PCB bow-tie antenna array for (77-81) GHz radar applications. *IEEE Transactions on Antennas and Propagation*, 68(3), 2379-2386. https://doi.org/10.1109/TAP.2019.2949723
- Pimentel, J. R. (2017). Data heterogeneity, characterization, and integration in the context of autonomous vehicles. IECON 2017 43rd Annual Conference of the IEEE Industrial Electronics Society, Beijing, China.
- Saleem, M. K., Vettikaladi, H., Alkanhal, M. A., & Himdi, M. (2017). Lens antenna for wide angle beam scanning at 79 GHz for automotive short range radar applications. *IEEE Transactions on Antennas and Propagation*, 65(4), 2041-2046. https://doi.org/10.1109/TAP.2017.2669726
- Wang, X., & Stelzer, A. (2013). A 79-GHz LTCC patch array antenna using a laminated waveguide-based vertical parallel feed. *IEEE Antennas and Wireless Propagation Letters*, 12, 987-990. https://doi.org/10.1109/LAWP.2013.2276756
- Yin, J., Wu, Q., Yu, C., Wang, H., & Hong, W. (2017). Low-Sidelobe-Level Series-Fed Microstrip Antenna Array of Unequal Interelement Spacing. IEEE Antennas and Wireless



Propagation Letters, 16, 1695-1698. https://doi.org/10.1109/LAWP.2017.2666427

Yoo, S., Milyakh, Y., Kim, H., Hong, C., & Choo, H. (2020). Patch array antenna using a dual coupled feeding structure for 79 GHz automotive radar applications. *IEEE Antennas and Wireless Propagation Letters*, 19(4), 676-679. https://doi.org/10.1109/LAWP.2020.2976545